Supporting Information

Minyan Zhong[1], Mark Simons[1], Lijun Zhu[1], Brent Minchew[2]

[1]California Institute of Technology, Pasadena, CA, U.S.

[2]Massachusetts Institute of Technology, Cambridge, MA, U.S.

Contents of this file

1. Text S1 to S10

2. Figures S1 to S12

Additional Supporting Information (Files uploaded separately)

1. Captions for Datasets S1

2. Captions for Movies S1 to S3

Text S1. Synthetic Test of the Linear Model

We discuss the results of the optimal model for no-grounding (Figure S1 and Figure S2) and grounding scenarios (Figure S3 and Figure S4). In the no-grounding scenario, the bias of amplitude estimation for M_2, N_2, O_1, and M_{sf} is less than 5 cm. Bias in the phase estimation of M_2 is close to zero; for N_2, there is an approximately +20 min bias uniformly across the entire ice shelf; for O_1, there is approximately +20 min bias on the upstream half of the ice shelf except the western and eastern margins. Near the southern end of the area of observation where the available viewing angles are limited, the bias in the estimation can increase. In the grounding scenario, the estimates of the vertical displacement for M_2, N_2, and O_1 has moderate difference when compared with the no-grounding scenario. The estimated amplitude of these three are systematically underestimated and has bias at -20 cm, -10 cm, and -5 cm, respectively. For the phase estimation, there is an approximately 10 min bias for M_2, an approximately +20 min bias for N_2, and an approximately +40 min bias for O_1 in upstream half similar to no-grounding scenario. Due to the grounding, the amplitude of the key vertical M_{sf} increases from less than 5 cm in the no-grounding scenario to approximately 25 cm. The two synthetic tests show that the vertical displacement at M_2, N_2, and O_1 can be well estimated. More importantly, they demonstrate that the vertical M_{sf} constituent can serve as a diagnostic proxy for the existence of ephemeral grounding.

Text S2. Formulation of the Linearized Inverse Problem

Let $E(t) = \max(\sum_\xi \tilde{a}_\xi \sin(\omega_\xi t + \phi_\xi), K'(\mathbf{r}))$, then we can write the up component of

displacement vector as

$$\begin{bmatrix} \Delta u_1^{\hat{u}} \\ \Delta u_2^{\hat{u}} \\ \vdots \\ \Delta u_q^{\hat{u}} \end{bmatrix} = \begin{bmatrix} \Delta t_1 \\ \Delta t_2 \\ \vdots \\ \Delta t_q \end{bmatrix} v^{\hat{u}} + \begin{bmatrix} E(t_1^b) - E(t_1^a) \\ E(t_2^b) - E(t_2^a) \\ \vdots \\ E(t_q^b) - E(t_q^a) \end{bmatrix} A. \tag{1}$$

We can arrive at the form of the linear inverse problem for the remaining parameters naturally combining the linear form of all three components and projecting the displacement vectors onto the observational unit vectors:

$$\mathbf{d} = \mathbf{G}'\mathbf{m}' \tag{2}$$

where $\mathbf{d}$ is observed displacement, the $\mathbf{G}'$ is the design matrix, and $\mathbf{m}'$ includes all parameters except K. We can find the optimal model using the closed-form solutions

$$\tilde{\mathbf{m}'} = (\mathbf{G}'^T\mathbf{C}_\chi^{-1}\mathbf{G}' + \mathbf{C}_{m'}^{-1})^{-1}\mathbf{C}_\chi^{-1}\mathbf{G}'^T\mathbf{d} \tag{3}$$

$$\tilde{\mathbf{C}}_{m'} = (\mathbf{G}'^T\mathbf{C}_\chi^{-1}\mathbf{G}' + \mathbf{C}_{m'}^{-1})^{-1} \tag{4}$$

where $\mathbf{C}_{m'}$ is the prior model covariance matrix for parameters expect K.

Text S3. The Computation of Credible Interval

We calculate the highest posterior density interval (HPDI) as the credible interval. The formal definition of HPDI is as follows:

Let $f(x)$ be the density function of a random variable X. Then the $100(1-\alpha)\%$ HPDI is the subset $R(f_\alpha)$ of the sample space of X such that

$$R(f_\alpha) = \{x : f(x) \geq f_\alpha\} \tag{5}$$

where f_α is the largest constant such that $P(X \in R(f_\alpha)) \geq 1 - \alpha$.

In our case X is the ephemeral grounding level K' defined on the real line and $\alpha = 0.05$. We use the measure of $100(1-\alpha)\%$ HPDI on the real line as the size of the credible interval.

Text S4. Formal Errors in the Synthetic Test of the Nonlinear Model

The formal errors in the synthetic tests of the nonlinear model are in Figure S5.

Text S5. Additional Results Inferred from the Linear Model

The additional results from the linear model are in Figure S6 and S7.

Text S6. Discussion of Vertical Amplitude Scaling $A(\mathbf{r})$

We present a discussion on the displacement amplitude of vertical M_2, N_2, and O_1 as well as the motivation of the using a lumped parameter $A(\mathbf{r})$ to describe the amplitude variation of all tidal constituents. Figure S8a-c show the normalized spatial variation in amplitude of vertical M_2, N_2 and O_1, calculated by dividing the inferred amplitude $a(\mathbf{r})$ by the amplitude at the reference point $a(\mathbf{r}_0)$ (Figure 1b). M_2, N_2 and O_1 demonstrate similar normalized spatial variation in amplitude ($a(\mathbf{r})/a(\mathbf{r}_0)$) with the difference between every two tidal constituents shown in Figure S8d-f. Thus, we make an empirical assumption that all tidal constituents share similar normalized spatial variation in amplitude and use a lumped parameter $A(\mathbf{r})$ to describe this spatial variation. The use of $A(\mathbf{r})$ enables the linearization of the nonlinear inverse problem.

The inferred $A(\mathbf{r})$ is mainly constrained by the major semi-diurnal constituents (e.g., M_2) because they are a few time larger in amplitude than the major diurnal constituents (e.g, O_1). The difference in normalized amplitude between the two semidiurnal constituents (M_2 and N_2) and the diurnal constituent O_1 is $\sim$0.1. Given the amplitude of two major diurnal constituents K_1 and O_1 is approximately 35 cm, the mean error of ignoring the possible difference between the amplitude variation of semi-dirunal and dirunal constituents translates to be only $\sim$5 cm. This is a few times smaller than the sum of measurement error and modeling error in data which is typically larger than 20 cm.

Text S7. Construction of the Nonlinear Vertical Displacement Model

We derive the relative spatial phase variations for M_2, N_2, and O_1 which inform the relative phase variation of the other 5 semi-diurnal and diurnal variations. Because the inferred phase maps for these three contains the bias in estimation, spurious phase variation caused by the ephemeral grounding and noise, we apply the following post-processing procedures on the original inferred maps and then obtain the relative phase variation (Figure S9):

1. Correct for the bias estimated by the synthetic test.

2. Remove the phase variation related to the ephemeral grounding including the isolated ephemeral grounding zone in central trunk and the low-amplitude node on the west margin.

3. Apply median filter (7x7) to further reduce the noise.

4. Calculate phase difference relative to the reference point.

Because the only strong phase variation in O_1 phase map has the similar shape and magnitude as the synthetic test (Figure S1), we simply assume that there is no phase variation in O_1.

The spatial amplitude variation of each constituent is defined as its amplitude at the reference point $\tilde{a_\xi}(\mathbf{r}_0)$ multiplied by the spatial scaling parameter $A(\mathbf{r})$. Same as the phase, we use the measured amplitude value at reference point for M_2, N_2, and O_1, and CATS2008 amplitude value for the rest.

Text S8. Derived Grounding Line from M_2 Displacement Amplitude

We derive updated grounding line at Rutford Ice Stream using the 10 cm contour of M_2 vertical displacement amplitude. The updated grounding line has better accuracy at the two horns of the grounding line and on the western margin of the ice shelf (Figure S10).

Text S9. Additional Results Inferred from the Nonlinear Model

The additional results from the linear model. Figure S11 shows the secular velocity. Figure S12 shows the formal error in the inferred secular velocity and tide-induced displacements. Figure S13 shows the inferred extent of ephemeral grounding from using different upper bounds of the credible interval size.

Text S10. Estimation of Variation in Longitudinal Stress

Here, we derive a physical model for the response to periodic forcing of laterally confined ice streams employing a Maxwell viscoelastic rheology for ice and applying small perturbations with sub-annual periods in longitudinal stress.

We derive the model in a righthand coordinate system oriented such that x is parallel to the horizontal component of the glacier flow vector u, y is oriented across flow (in the horizontal plane) with $y = 0$ at the centerline, and z points up with $z = 0$ at the bed.

The consituitive relation for a Maxwell viscoelastic material is given as

$$2\eta\dot{\epsilon}_{xx} = \tau_{xx} + T_r\dot{\tau}_{xx} \tag{6}$$

where $T_r = \eta/E$ is the relaxation time, $\dot{\epsilon}_{xx} = \partial u/\partial x$ is the longitudinal (normal) strain rate, τ_{xx} is the longitudinal deviatoric stress, and over-dots indicate time derivatives (e.g., $\dot{\tau}_{xx} = \partial\tau_{xx}/\partial t$). The non-Newtonian viscosity of ice is defined as

$$\eta = \mu\dot{\epsilon}_e^{1/n-1} \tag{7}$$

$$\mu = \frac{1}{2A^{1/n}} \tag{8}$$

$$\dot{\epsilon}_e = \sqrt{\dot{\epsilon}_{ij}\dot{\epsilon}_{ij}/2} \tag{9}$$

$$\dot{\epsilon}_{ij} = \frac{1}{2}(\frac{\partial u_i}{\partial x_j} + \frac{\partial u_j}{\partial x_i}) \tag{10}$$

where $\dot{\epsilon}_{ij}$ is a component of the strain rate tensor, $\dot{\epsilon}_e$ is the effective strain rate, A is the creep parameter along the centerline of the ice stream, and n is the exponent in the Nye-Glen flow law. We assume both n and A are constant hereafter.

Our interest is the frequency response of ice streams to small perturbations in longitudinal stress. We therefore consider periodic variations in longitudinal stress as

$$\tau_{xx} = \bar{\tau}_{xx} + \hat{\tau}_{xx} e^{i(-\omega t + kx)} \tag{11}$$

where kx, ω is the angular wavenumber, $i^2 = -1$, over-bars represent secular (i.e., time-invariant) terms, and hats represent complext coefficients of periodic variations. Similaly, we take flow speed to be of the form

$$u = \bar{u} + \hat{u}_{xx} e^{i(-\omega t + kx)} \tag{12}$$

. For small perturbations, we impose $|\hat{\tau}_{xx}| \ll |\bar{\tau}_{xx}|$ and assume $|\hat{u}| \ll |\bar{u}|$.

To simplify our analysis, we consider the viscoelastic relaxation time T_r to be an intrinsic material property that remains constant in time. In other words, we assume that, following a step change in strain, stress decays exponentially in time with a constant relaxation (e-folding) time, hereafter designated $\bar{T}_r$. To reflect this assumption, we replace the visoelastic relaxation time T_r in equation (6) with

$$\bar{T}_r = \frac{\bar{\eta}}{E} \tag{13}$$

where

$$\bar{\eta} = \mu (\frac{\partial \bar{u}}{\partial x})^{1/n-1} \tag{14}$$

is the secular component of the effetive dynamic viscosity and E is assumed constant in space and time.

Combining equations (6) to (13) to relate the coefficients of periodic variations in longitudinal stress and speed yields

$$\frac{\hat{\tau}_{xx}}{\hat{u}} = \frac{2\bar{\eta}k}{n}\left(\frac{-\mathrm{De}+i}{1+\mathrm{De}^2}\right) \tag{15}$$

where $\mathrm{De} = \omega\bar{T}_r$ is the real-valued, positive, dimensionless Deborah number, which is proportional to the ratio of the viscoeslatic relaxation time to be forcing period.

The observable angular wavenumber is

$$k = \frac{\omega}{v_p} + i\frac{1}{l} \tag{16}$$

where ω is angular frequency of the flow rate variation, v_p is the phase velocity of the upstream propagation, and l is the upstream decay distance in amplitude.

At RIS, the inferred fortnightly flow variability in Minchew et al., (2017) and this study both indicate $\omega = 2\pi/14.7\,\mathrm{day}$, $l = 45\,\mathrm{km}$, and $v_p = 24\,\mathrm{km/d}$. We further assume the relaxtion time $\bar{T}_r \approx 10\,\mathrm{days}$ at RIS which is consistent with the typical values of $\hat{\eta} \sim 10^{15}\ \mathrm{Pa}\cdot\mathrm{S}$ and $E \sim 10^9\ \mathrm{Pa}$ (Cuffey and Paterson, 2010) and the observation at RIS.

Plugging in these values and $\hat{u} = 0.2\mathrm{m/d}$, $n = 4$ (Millstein et al., 2022) into equation (15), the estimated $\hat{\tau}_{xx}$ is approximately $75\,\mathrm{KPa}$.

Dataset S1. Updated Grounding Line of Rutford Ice Stream

We provide the grounding line data of Rutford Ice Stream as Dataset S1 in the format of ASCII text data. The data consists of the points delineating the grounding line in geographic coordinates (latitude and longitude). In the text file, each row indicate the coordinate of a point in the order of longitude and latitude.

Movie S1. Vertical Displacement and Ephemeral Grounding at Rutford Ice Stream

Movie S2. Fortnightly Variation in Horizontal Flow Rate and Areal Strain Rate at Rutford Ice Stream

Movie S3. Centerline Along-Flow Fortnightly Flow-Rate Variation at Rutford Ice Stream

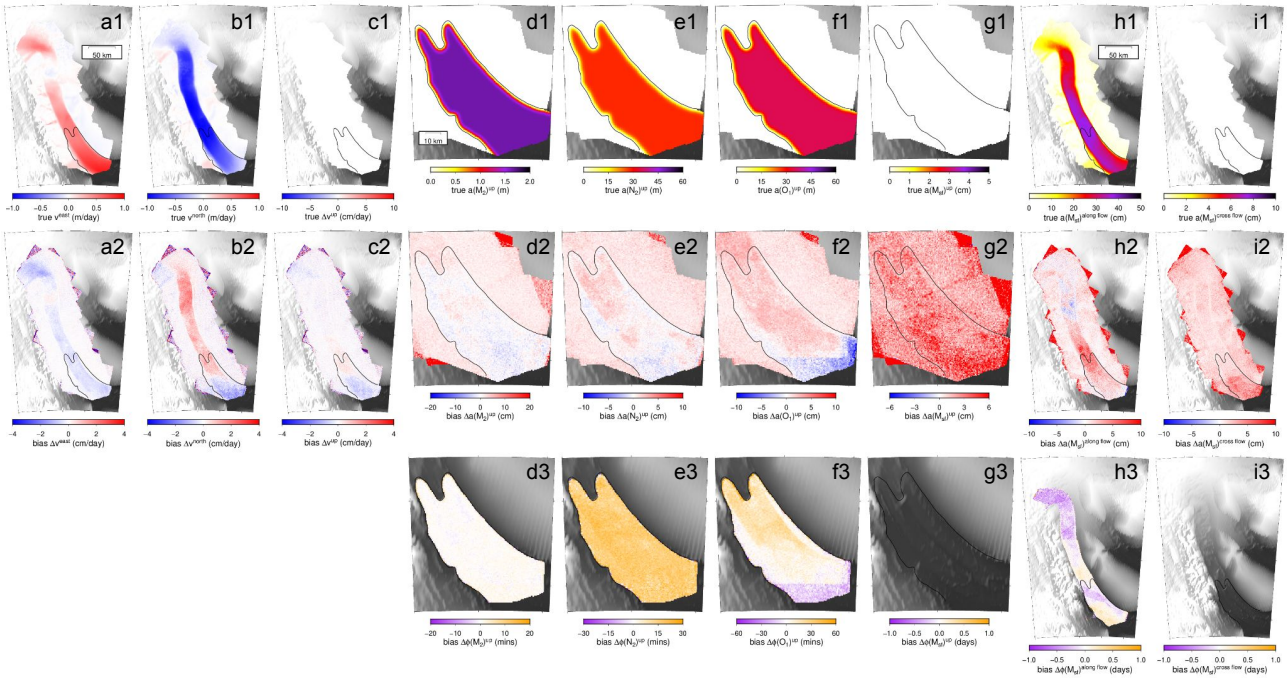

Figure S1. Input and the bias of estimated secular and tide-induced displacement using the linear model when there is no ephemeral grounding. (a1-c1) Input secular horizontal and vertical velocity. (d1-g1) Input amplitude of vertical sinusoidal displacement at M_2, N_2, O_1, and M_{sf} period. (h1-i1) Input amplitude of horizontal sinusoidal displacement at M_{sf} period. Input phases of all sinusoidal displacement are spatially constant and are not shown. The bias of estimation is defined as the inferred value minus the input value. (a2-c2) Bias of estimated secular velocity. (d2-g2) Bias of estimated amplitude of vertical sinusoidal displacements. (d3-g3) Bias of estimated phase of sinusoidal vertical displacements. (h2-i2) Bias of estimated amplitude of horizontal sinusoidal displacement. (h3-i3) Bias of estimated of phase of horizontal sinusoidal displacement. Phase estimates which correspond to small amplitude estimates and large uncertainties are not shown.

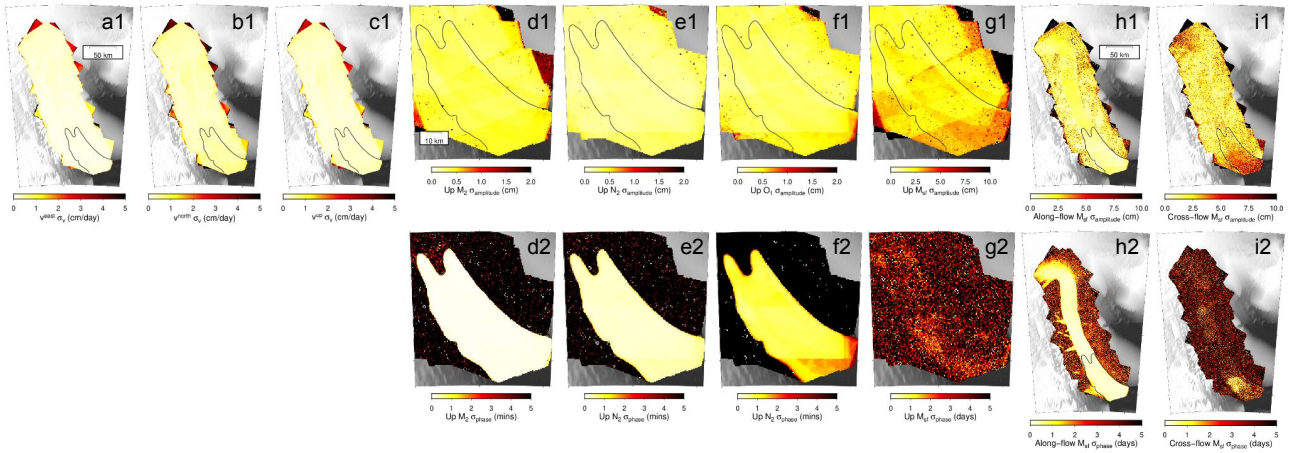

Figure S2. Formal errors in estimated secular velocity, vertical displacement, and horizontal displacement variations in the synthetic test without ephemeral grounding inferred by the linear model. (a1-c1) Standard deviation of estimated secular east, north, up velocity. (d1-g1) Standard deviation of estimated vertical displacement amplitude at M_2, N_2, O_1, M_{sf} periods. (h1-i1) Standard deviations of along-flow and cross-flow displacement amplitude at M_{sf} period. (d1-g1) Standard deviation of estimated vertical displacement amplitude at M_2, N_2, O_1, M_{sf} periods. (h2-i2) Standard deviation of estimated along-flow and cross-flow displacement phase at M_{sf} period.

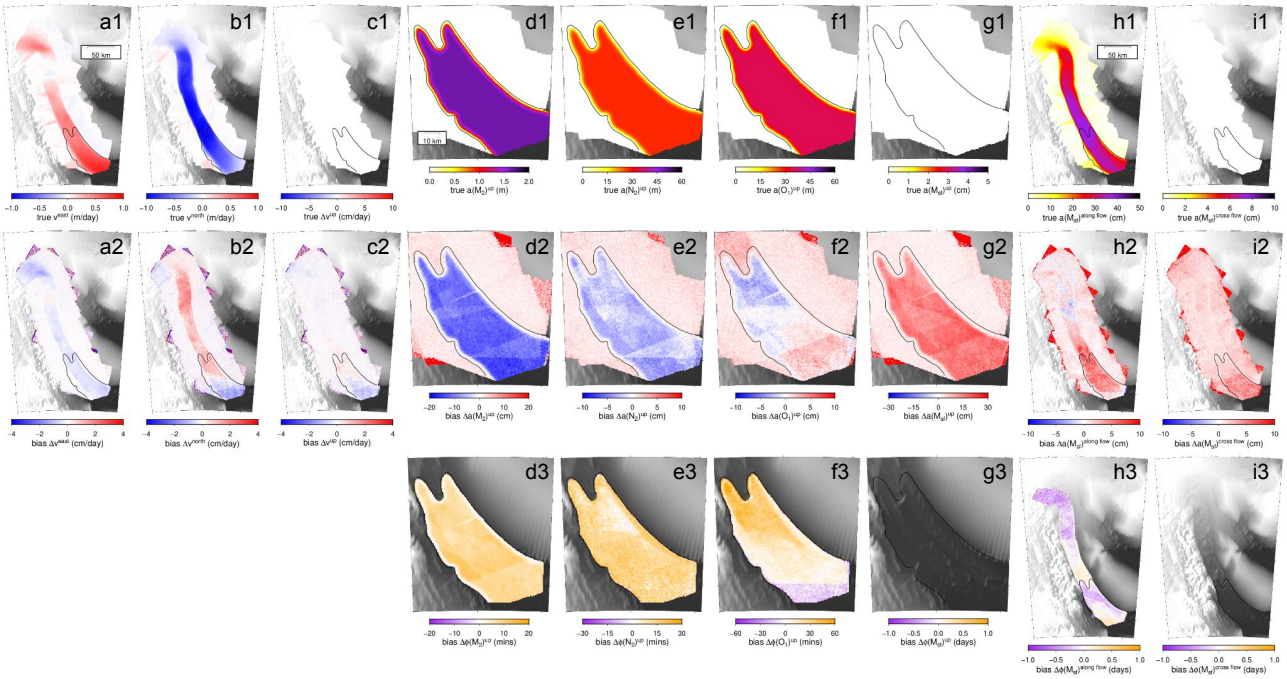

Figure S3. Input and the bias of estimated secular and tide-induced displacement using the linear model assuming the seafloor is 1.5 m beneath the ice shelf. Ephemeral grounding occurs when the low tide is smaller than −1.5 m. The layout of the panels is the same as Figure S1.

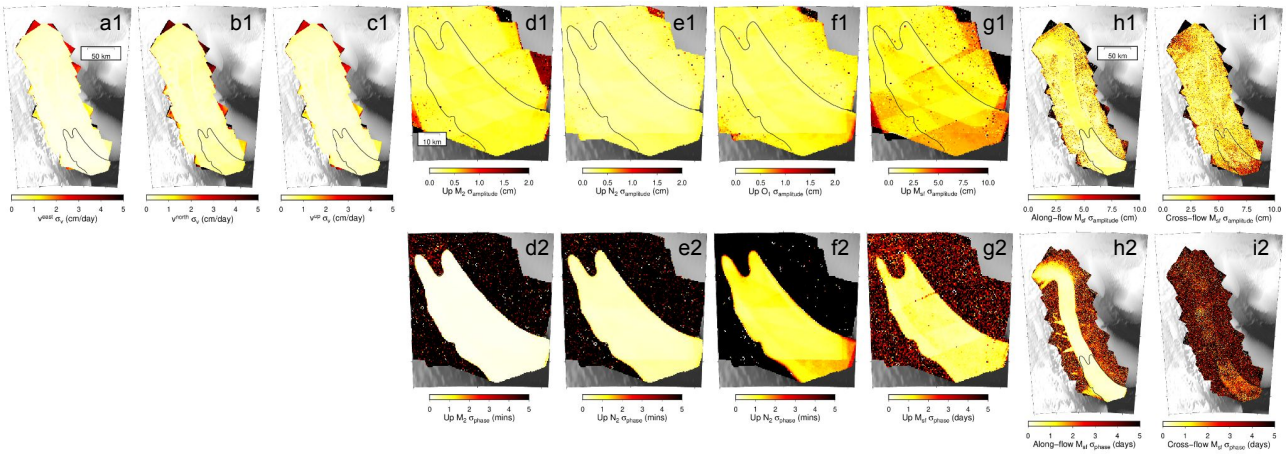

Figure S4. Formal errors in estimated secular velocity, vertical displacement, and horizontal displacement variations in the synthetic test with ephemeral grounding inferred by the linear model. The layout of the panels is the same as Figure S2.

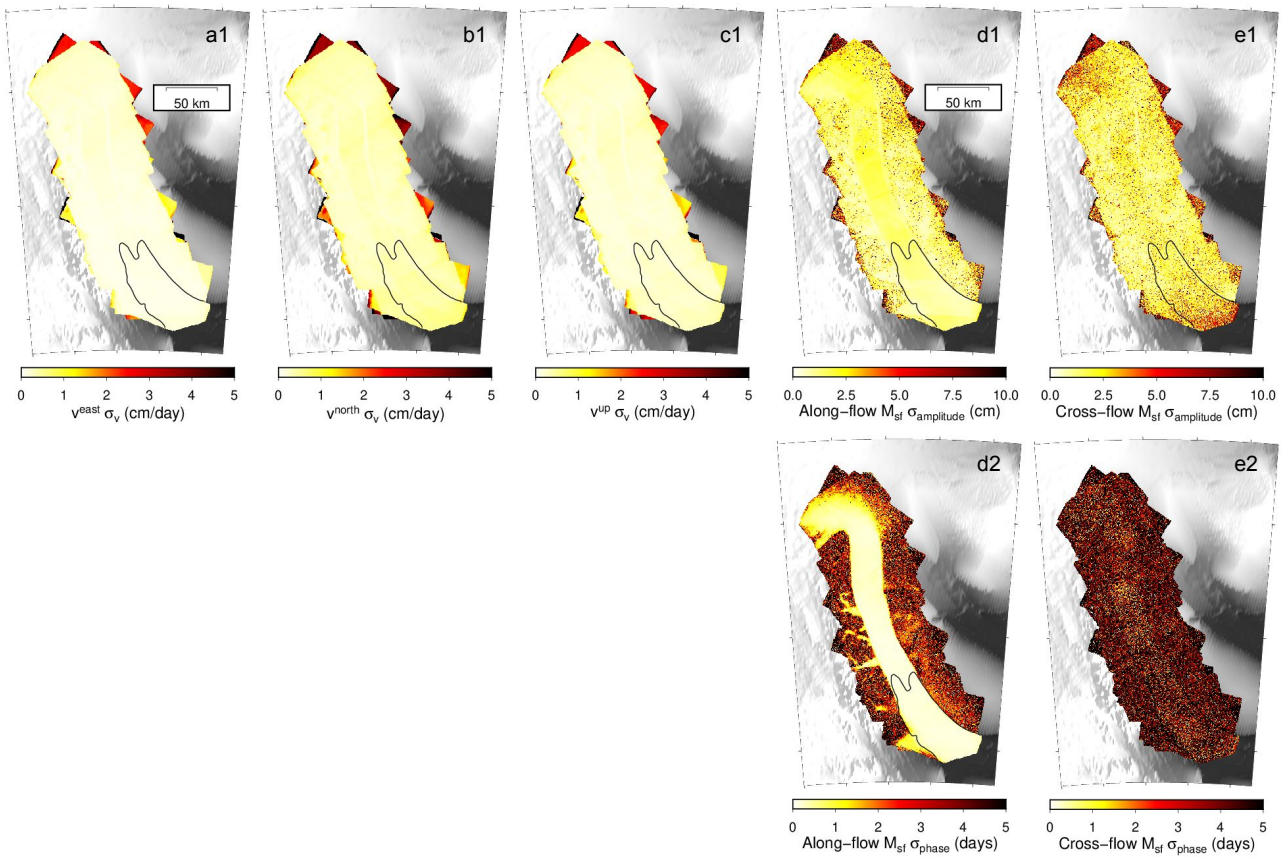

Figure S5. Formal errors in the synthetic test of the nonlinear model. (a1-c1) Standard deviation of estimated secular east, north, up velocity. (d1-e1) Standard deviations of along-flow and cross-flow displacement amplitude at M_{sf} period. (d2-e2) Standard deviation of estimated along-flow and cross-flow displacement phase at M_{sf} period.

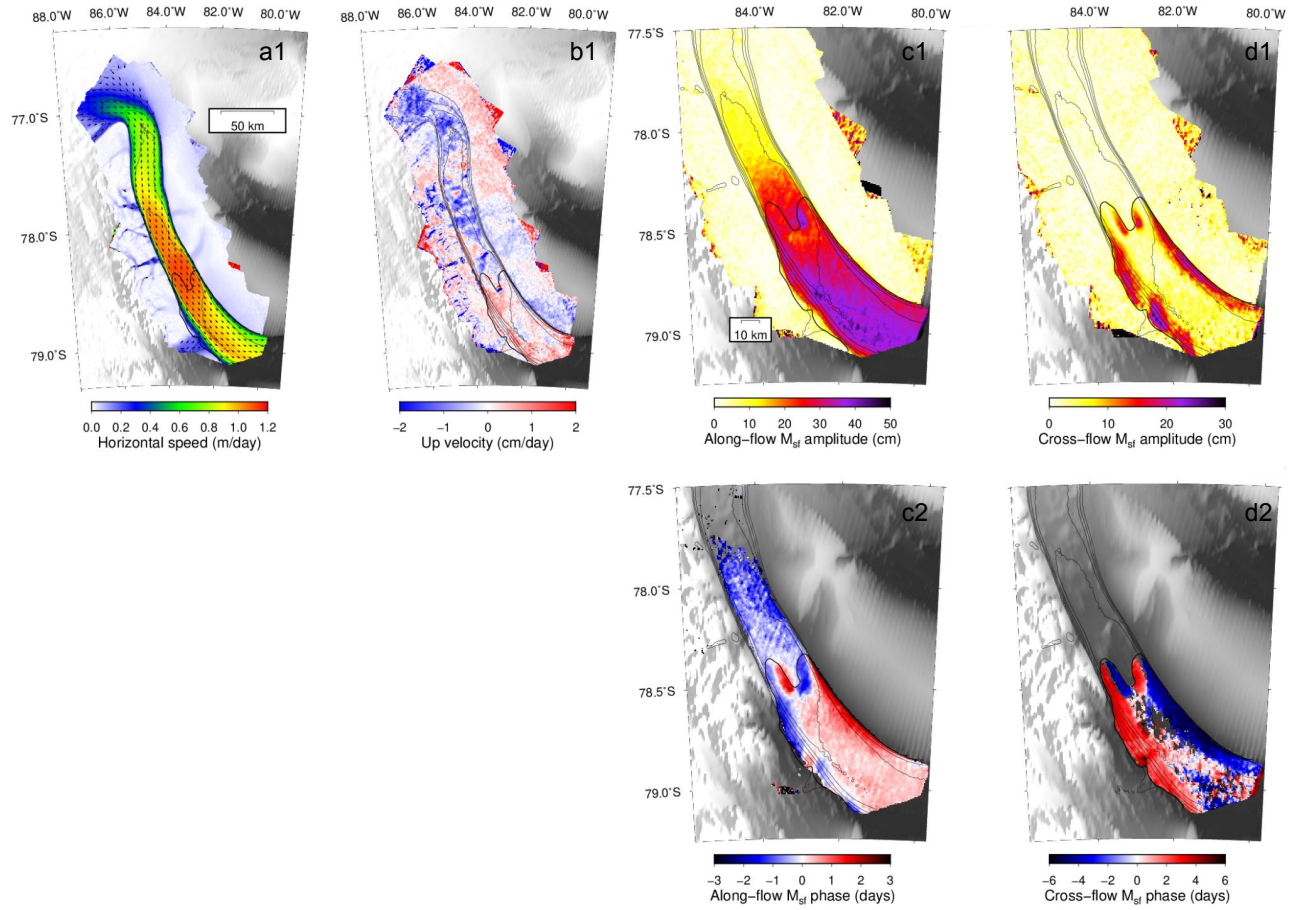

Figure S6. (a1) Horizontal velocity where the color indicates speed and arrows show flow direction (b1) Vertical velocity, where the positive values indicate moving upward. (c1-d1) The amplitude of horizontal displacement variation at M_{sf} period. (c2-d2) The phase of horizontal displacement variation at M_{sf} period.

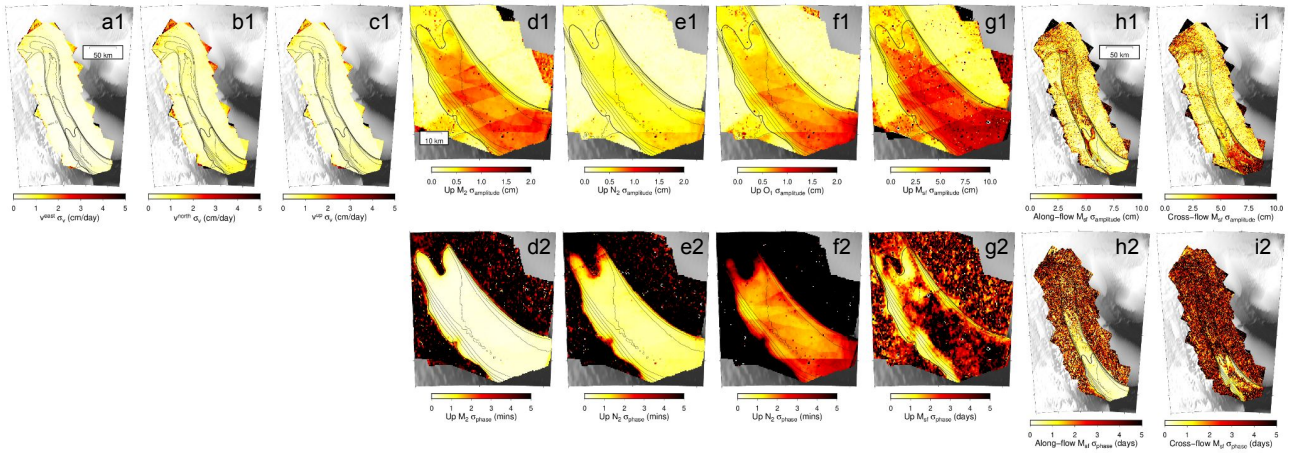

Figure S7. Formal errors in estimated secular velocity, vertical displacement and horizontal displacement variations by the linear model. (a1-c1) Standard deviation of estimated secular east, north, up velocity. (d1-g1) Standard deviation of estimated vertical displacement amplitude at M_2, N_2, O_1, M_{sf} periods. (h1-i1) Standard deviations of along-flow and cross-flow displacement amplitude at M_{sf} period. (d1-g1) Standard deviation of estimated vertical displacement amplitude at M_2, N_2, O_1, M_{sf} periods. (h2-i2) Standard deviation of estimated along-flow and cross-flow displacement phase at M_{sf} period.

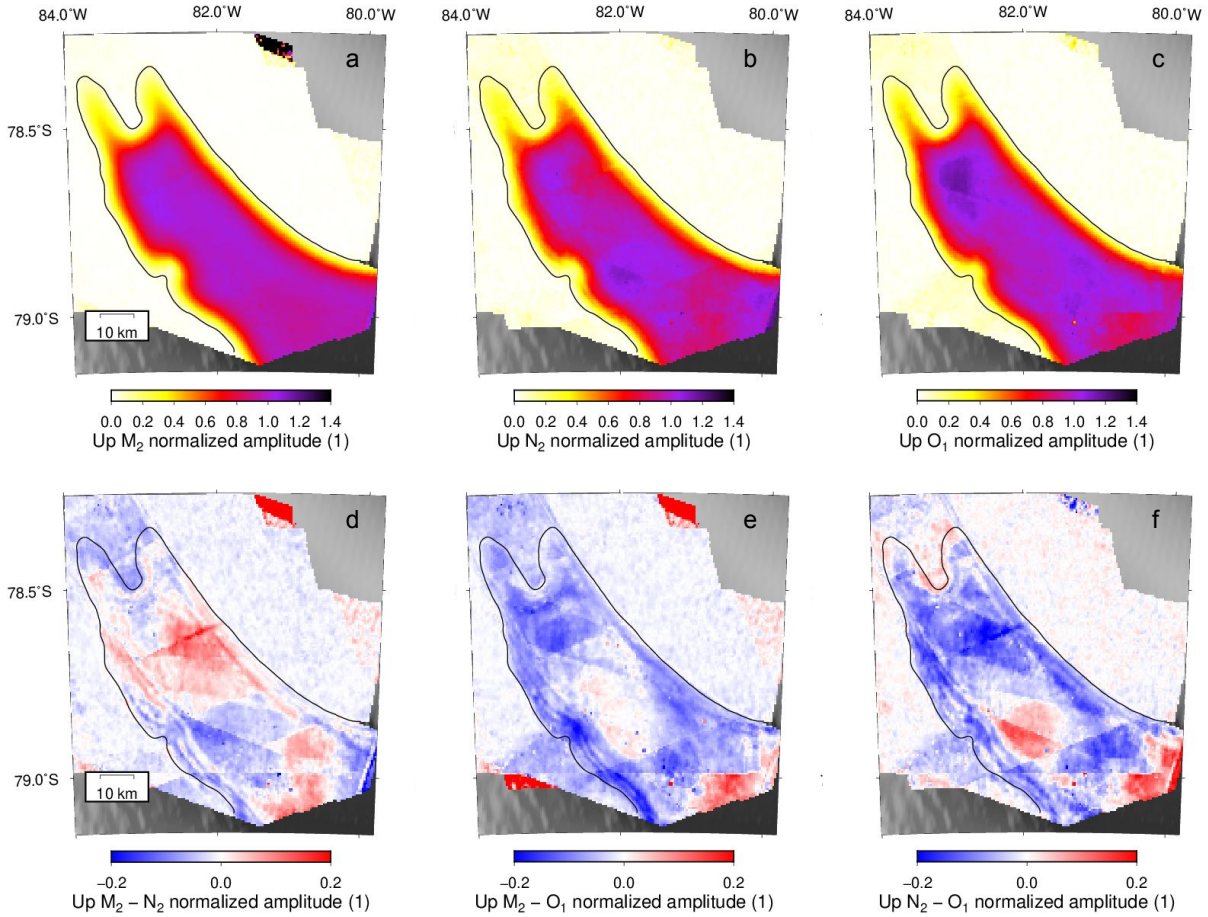

Figure S8. (a-c) The normalized displacement amplitude of vertical M_2, N_2 and O_1. (d-f) The difference of normalized displacement amplitude between M_2, N_2 and O_1.

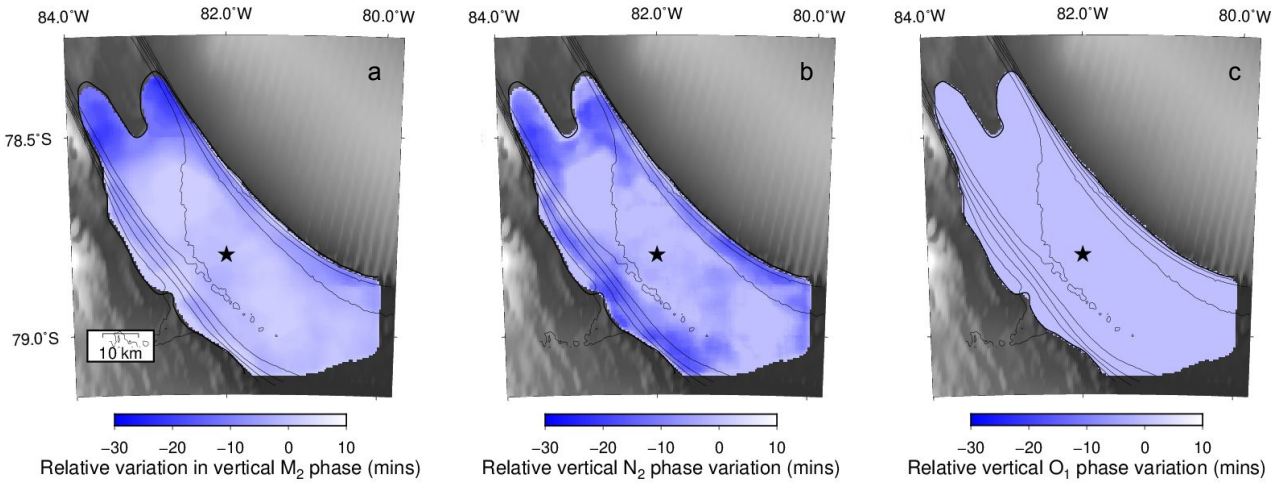

Figure S9. The relative phase variation of M_2, N_2, and O_1 derived from the result inferred by the linear model.

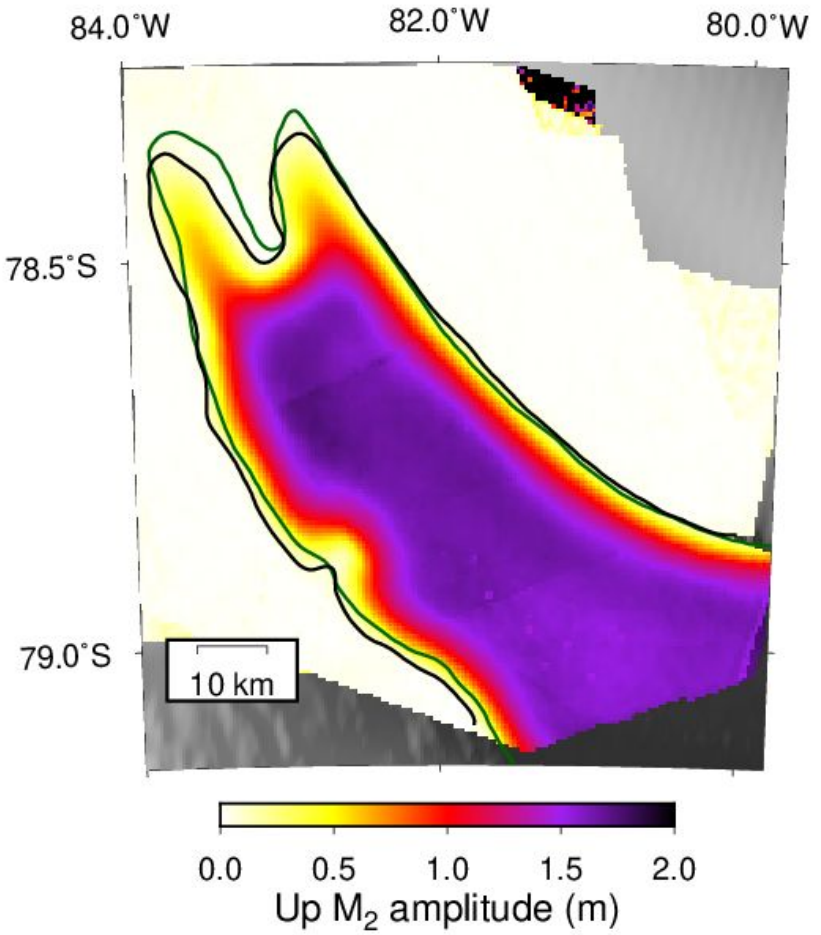

Figure S10. Grounding line at Rutford Ice Stream. Grounding line derived from M_2 displacement amplitude is in black. Grounding line from Bedmap2 (Fretwell et al., 2013) is in green.

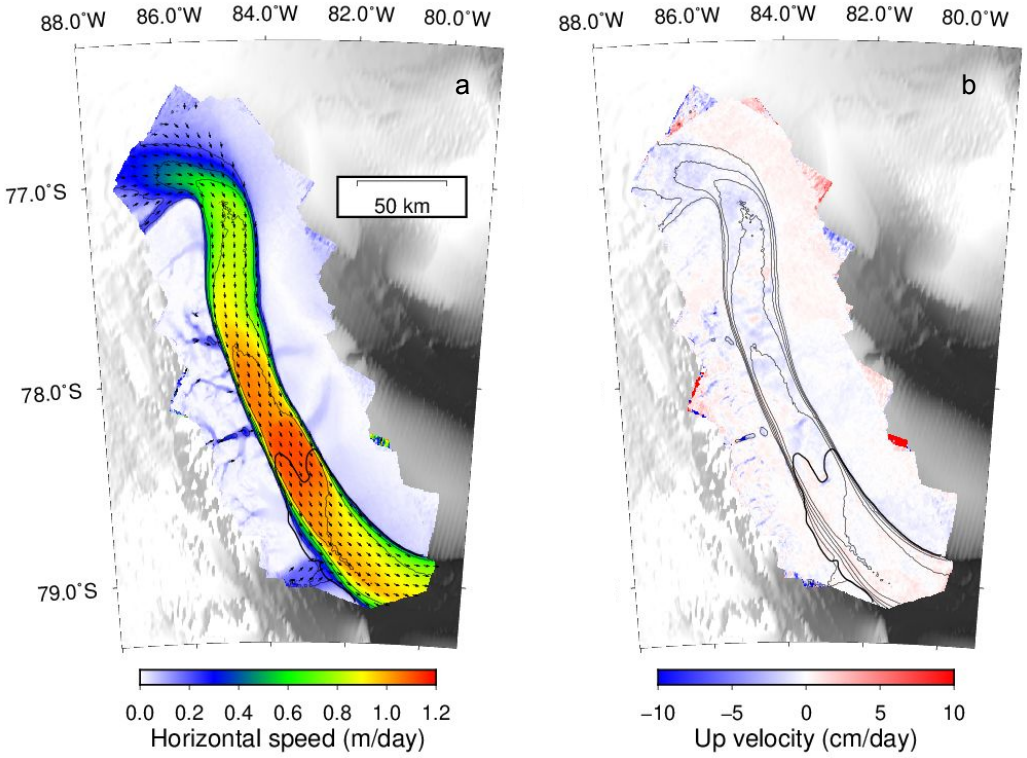

Figure S11. (a) Horizontal velocity where the color indicates speed and arrows show flow direction (b) Vertical velocity, where the positive values indicate moving upward.

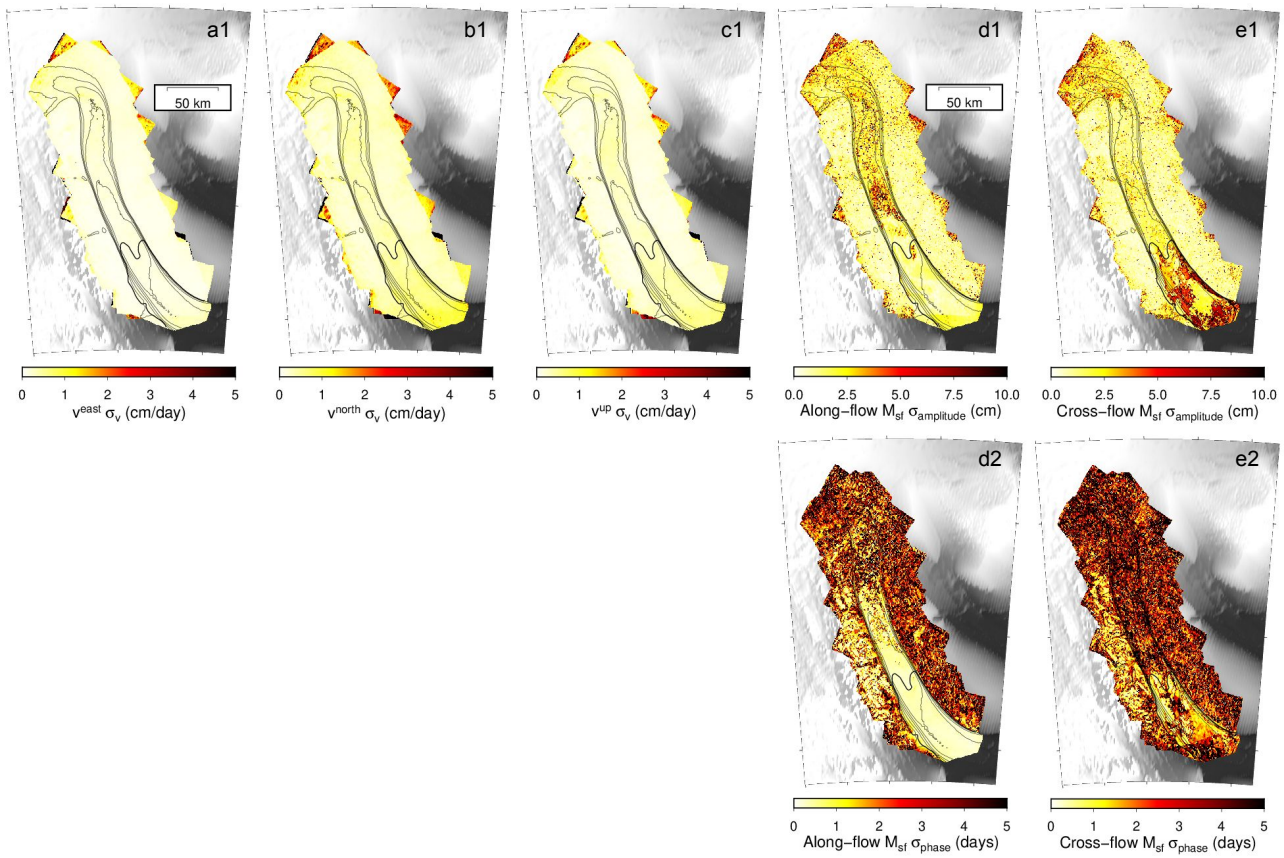

Figure S12. Formal errors in the synthetic test of the nonlinear model. (a1-c1) Standard deviation of estimated secular east, north, up velocity. (d1-e1) Standard deviations of along-flow and cross-flow displacement amplitude at M_{sf} period. (d2-e2) Standard deviation of estimated along-flow and cross-flow displacement phase at M_{sf} period.

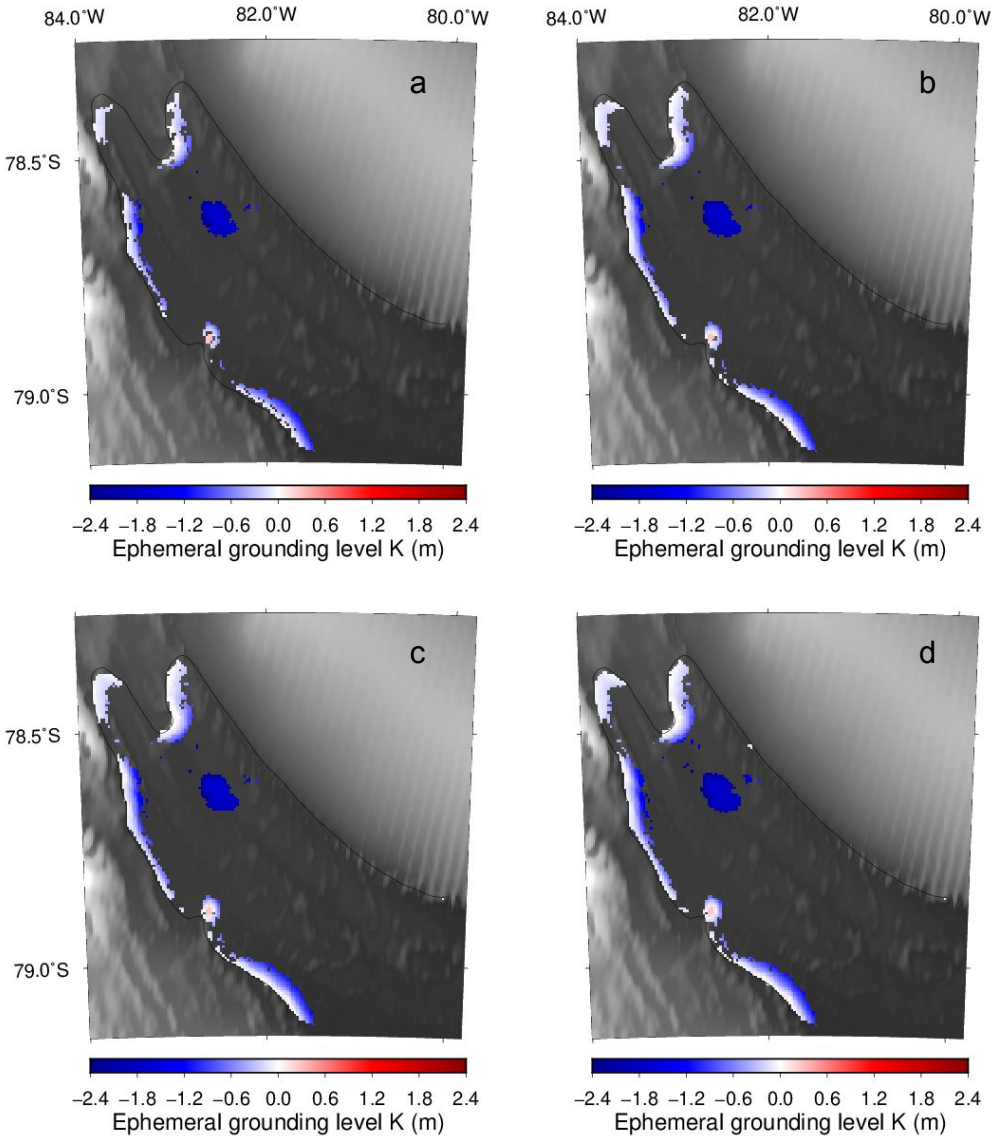

Figure S13. Inferred ephemeral grounding with different size of credible intervals. (a) credible interval size = 40 cm. (b) credible interval size = 60 cm. (c) credible interval size = 80 cm. (d) credible interval size = 100 cm.